

Complex saddles of the Veneziano amplitude

T. Yoda

Department of Physics, Kyoto University, Sakyo-ku, Kyoto 606-8502, Japan

E-mail: t.yoda@gauge.scphys.kyoto-u.ac.jp

ABSTRACT: Saddle point approximation is a useful method to explore high energy asymptotic behaviors of string scattering amplitudes. We show that, even at tree-level, there are infinitely many complex saddles contributing to string scattering amplitudes, and that the complex saddles reproduce their appropriate poles and zeros. Each complex saddle is interpreted as a semi-classical path of a string in Lorentzian signature. The poles and zeros of the Veneziano amplitude are understood as constructive or destructive interference of such semi-classical paths.

Contents

| | | |
|----------|--|-----------|
| 1 | Introduction | 1 |
| 2 | Veneziano amplitude and its real saddle | 3 |
| 2.1 | Veneziano amplitude | 3 |
| 2.2 | Real saddle | 4 |
| 3 | Complex saddles | 6 |
| 3.1 | Regularization of worldsheet integral | 6 |
| 3.2 | Complex saddles and thimble analysis | 6 |
| 4 | Discussions | 11 |
| 4.1 | Stringy excitations | 11 |
| 4.2 | Semi-classical paths | 12 |
| 4.3 | Unitarity and locality | 14 |
| 5 | Conclusion | 15 |
| A | Thimble analysis | 16 |
| A.1 | Gamma function | 16 |

1 Introduction

Scattering amplitude is one of the most fundamental subjects of study in physics. In particular, string scattering amplitudes and their higher genus corrections are of great interest in understanding quantum gravity. Exploring their high energy asymptotic behaviors has the potential to alter our understanding of spacetime.

Asymptotic behaviors of string scattering amplitudes have been studied by saddle point approximation method in [1–6]. On-shell string scattering amplitudes, with the fixed angle, were evaluated by the dominant saddle point at each perturbative order. Their Borel resummation exhibited a characteristic fall-off, which was interpreted as an improvement of locality while maintaining the ultraviolet finiteness of string scatterings [6].

One remaining problem of their saddle point analysis is whether there exist other saddle points that contribute to string scattering amplitudes. Also, one may wish to compute the angle dependence of string scattering amplitudes at the high energy limit. Since a string is a finite-sized object and its worldsheet can have nontrivial topology, string scatterings must be more erratic than the scatterings of point particles in perturbative QFTs. If such erratic behaviors could be evaluated quantitatively, one may approach the nature of spacetime at the Planck scale. Moreover, one may wish to analytically continue previous results of saddle point approximation to other kinematic regions. One possible way to analytically

continue is to use a formula of the gamma function as the authors of [7] used in order to reproduce the appropriate KLT formula [8] at the tree-level from the results of saddle point approximation in [1, 2]. However, it will be better to avoid using an explicit formula of the gamma function because we are not necessarily able to obtain an analytic expression for higher genus corrections in general.

The purpose of this paper is to answer these three questions. We start from the tree-level case, namely the Veneziano amplitude [9], expecting that our analysis can be extended to higher genus corrections in future works. Our results show that there exist infinitely many complex saddles hidden in different Riemann sheets contributing to string scattering amplitudes. The contributions from infinitely many complex saddles reproduce the appropriate angle dependence, and the appropriate poles and zeros of the amplitude. The location of the poles and zeros agrees with the result of analytic continuation obtained from the reflection formula of the gamma function.

We also show that the infinitely many complex saddles have physical significance. They are never technical artifacts of approximation and regularization. The infinitely many complex saddles we have found reproduce the appropriate poles and zeros, which are associated with the tower of stringy excitations. Each saddle is also interpreted as a semi-classical path of a string in Lorentzian signature, and the poles and zeros are understood as constructive or destructive interference of such semi-classical paths of a string. Moreover, the residue of each pole is consistent with partial wave unitarity.

Throughout our analysis, we have not collected complex saddle contributions by hand to reproduce the appropriate formula of the Veneziano amplitude. Rather, we have analyzed the thimble (steepest descent) structure of regularized worldsheet integral for the Veneziano amplitude, and found a specific class of complex saddles which contribute to the string amplitude. Also, our results are not inconsistent with the previous results of saddle point approximation [1–7, 10]. Contributions from complex saddles we have found do not change the universal fall-off in the asymptotic region, but give extra information about poles and zeros, in other words, about analytic continuation to different kinematic parameter regions.

It will be worthwhile to generalize our analysis to higher genus corrections. The authors of [1, 2] used an analogy of electromagnetism on a worldsheet to identify the dominant real saddle at each perturbative order. Our results will not ruin their analogy but rather be understood as a natural extension of it. Thus, we hope that our analysis is extended to higher orders to find analytic continuation and to make the unitarity of string scatterings manifest. Also, it will be necessary to study how modular invariance is reflected in complex saddles. Although we have found that complex saddles are associated with stringy excitations at the tree-level, it is still unclear how complex saddles can know other characteristic properties of a string. Such problems are left for future works.

This paper is organized as follows. In Sec. 2, we briefly review the Veneziano amplitude and its saddle point approximation. Then, we point out that the dominant real saddle does not know the appropriate poles and zeros of the amplitude, namely the appropriate analytic continuation. In Sec. 3, we regularize the formal worldsheet integral for the Veneziano amplitude by using the Feynman- $i\epsilon$ prescription following [11]. Then, by deforming the integration contour of the regularized worldsheet integral, we find that infinitely many

complex saddles are hidden in different Riemann sheets. In Sec. 4, we discuss the physical interpretation of the complex saddles. Finally in Sec. 5, we conclude this paper.

2 Veneziano amplitude and its real saddle

In this section, we quickly review the Veneziano amplitude [9]. It has a formal integral representation on the worldsheet, and it has the dominant real saddle. However, the real saddle is insufficient to reproduce the appropriate poles and zeros of the amplitude. In the following discussions, we use conventions $\alpha'_{\text{open}} = 1/2$ and almost plus signature.

2.1 Veneziano amplitude

The Veneziano amplitude (st -part) is given by a combination of the gamma functions as

$$\mathcal{A}_{st} = \frac{\Gamma(-\alpha(s))\Gamma(-\alpha(t))}{\Gamma(-\alpha(s) - \alpha(t))}, \quad \alpha(x) = x/2 + 1. \quad (2.1)$$

Here, the Mandelstam variables are defined as

$$s = -(p_1 + p_2)^2 = 4(|\mathbf{p}|^2 - 2), \quad (2.2a)$$

$$t = -(p_1 + p_3)^2 = -4|\mathbf{p}|^2 \frac{1 - \cos \theta}{2}, \quad (2.2b)$$

$$u = -(p_1 + p_4)^2 = -4|\mathbf{p}|^2 \frac{1 + \cos \theta}{2}, \quad (2.2c)$$

where

$$p_1 = \begin{pmatrix} \sqrt{|\mathbf{p}|^2 - 2} \\ |\mathbf{p}| \\ 0 \end{pmatrix}, \quad p_2 = \begin{pmatrix} \sqrt{|\mathbf{p}|^2 - 2} \\ -|\mathbf{p}| \\ 0 \end{pmatrix}, \quad -p_3 = \begin{pmatrix} \sqrt{|\mathbf{p}|^2 - 2} \\ |\mathbf{p}| \cos \theta \\ |\mathbf{p}| \sin \theta \end{pmatrix}, \quad -p_4 = \begin{pmatrix} \sqrt{|\mathbf{p}|^2 - 2} \\ -|\mathbf{p}| \cos \theta \\ -|\mathbf{p}| \sin \theta \end{pmatrix}. \quad (2.3)$$

In this convention, we have

$$\alpha(s) + \alpha(t) + \alpha(u) = -1. \quad (2.4)$$

The gamma function $\Gamma(z)$ can be defined by the Euler integral for $\text{Re } z > 0$. It is analytically continued to the whole complex plane except non-positive integers. It is convenient to use the reflection formula

$$\Gamma(z)\Gamma(1-z) = \frac{\pi}{\sin \pi z}, \quad z \neq 0, \pm 1, \dots \quad (2.5)$$

for finding the residue of the poles. The Veneziano amplitude (2.1) has s -channel poles at

$$\alpha(s) = n + 1, \quad n = -1, 0, 1, \dots \quad (2.6)$$

Around the s -channel poles, we have

$$\mathcal{A}_{st} \sim \frac{\Gamma(n + 2 + \alpha(t))}{\Gamma(n + 2)\Gamma(1 + \alpha(t))} \frac{(-1)^{n+2}\pi}{\sin \pi \alpha(s)}. \quad (2.7)$$

The first factor gives the residue around the pole. The Veneziano amplitude (2.1) has not only poles but also zeros since it has a gamma function in the denominator. It exhibits oscillatory behavior in general since $\alpha(t)$ in the denominator depends on the scattering angle θ .

2.2 Real saddle

The Veneziano amplitude (2.1) can be derived from a worldsheet integral

$$\mathcal{A}_{st} \stackrel{\text{formal}}{=} \int_0^1 dz |z|^{-\alpha(s)-1} |1-z|^{-\alpha(t)-1}, \quad (2.8)$$

as standard textbooks explain.

This is actually a formal integral since the integral diverges when $\text{Re } \alpha(s) \geq 0$ or $\text{Re } \alpha(t) \geq 0$. It is common that this is regarded as an analytic continuation from a region where the integral is well-defined. However, such a region is unphysical since $\alpha(s) \sim 2|\mathbf{p}|^2$ is supposed to be negative so that the integral is well-defined. At this stage, we already have a conceptual problem that physical amplitude is not defined in the physical region $\alpha(s) \sim 2|\mathbf{p}|^2 > 0$, rather defined as an analytical continuation from unphysical region $\alpha(s) \sim 2|\mathbf{p}|^2 < 0$.

Even if we ignore such a conceptual problem, we encounter another problem, which is the main topic of this paper. Let us rewrite the integral as

$$\mathcal{A}_{st} \stackrel{\text{formal}}{=} \int_0^1 dz e^{-(\alpha(s)+1) \ln |z| - (\alpha(t)+1) \ln |1-z|}. \quad (2.9)$$

In the high energy limit, presumably, its saddle point approximation is valid. It has a unique real saddle

$$z_0 = \frac{\alpha(s) + 1}{\alpha(s) + \alpha(t) + 2}. \quad (2.10)$$

Formally performing the Gaussian integral around this real saddle, we have

$$\begin{aligned} \mathcal{A}_{st} &\stackrel{\text{formal saddle}}{\sim} \left(\frac{\alpha(u)^3}{\alpha(s)\alpha(t)} \right)^{-1/2} e^{-(\alpha(s)+1) \ln \alpha(s) - (\alpha(t)+1) \ln \alpha(t) - (\alpha(u)-1) \ln \alpha(u)} \\ &\sim (stu)^{-3/2} \exp \left[-\frac{1}{2} (s \ln s + t \ln t + u \ln u) \right]. \end{aligned} \quad (2.11)$$

This coincides with the formal asymptotic expansion of (2.1) by using the Stirling's formula. That is

$$\begin{aligned} \mathcal{A}_{st} &\stackrel{\text{formal Stirling}}{\sim} [\alpha(s)\alpha(t)\alpha(u)]^{-1/2} e^{-\alpha(s) \ln \alpha(s) - \alpha(t) \ln \alpha(t) - \alpha(u) \ln \alpha(u)} \\ &\sim (stu)^{-3/2} \exp \left[-\frac{1}{2} (s \ln s + t \ln t + u \ln u) \right]. \end{aligned} \quad (2.12)$$

Although these two formal results (2.11) and (2.12) are consistent, they miss the poles and zeros of the original amplitude (2.1) at $\alpha(s), \alpha(s) + \alpha(t) \in \mathbb{Z}_{\geq}$. As Fig. 1 shows, the formal asymptotic expansion misses s -channel poles and oscillatory behavior around $\theta = \pi/2$ of the Veneziano amplitude, while the size of the amplitude is roughly the same.

The reason why we have missed the poles and zeros in (2.12) is because we have inappropriately used Stirling's formula:

$$\ln \Gamma(z) \sim (z - 1/2) \ln z - z + \ln \sqrt{2\pi} + \mathcal{O}(z^{-1}) \quad |\arg z| < \pi. \quad (2.13)$$

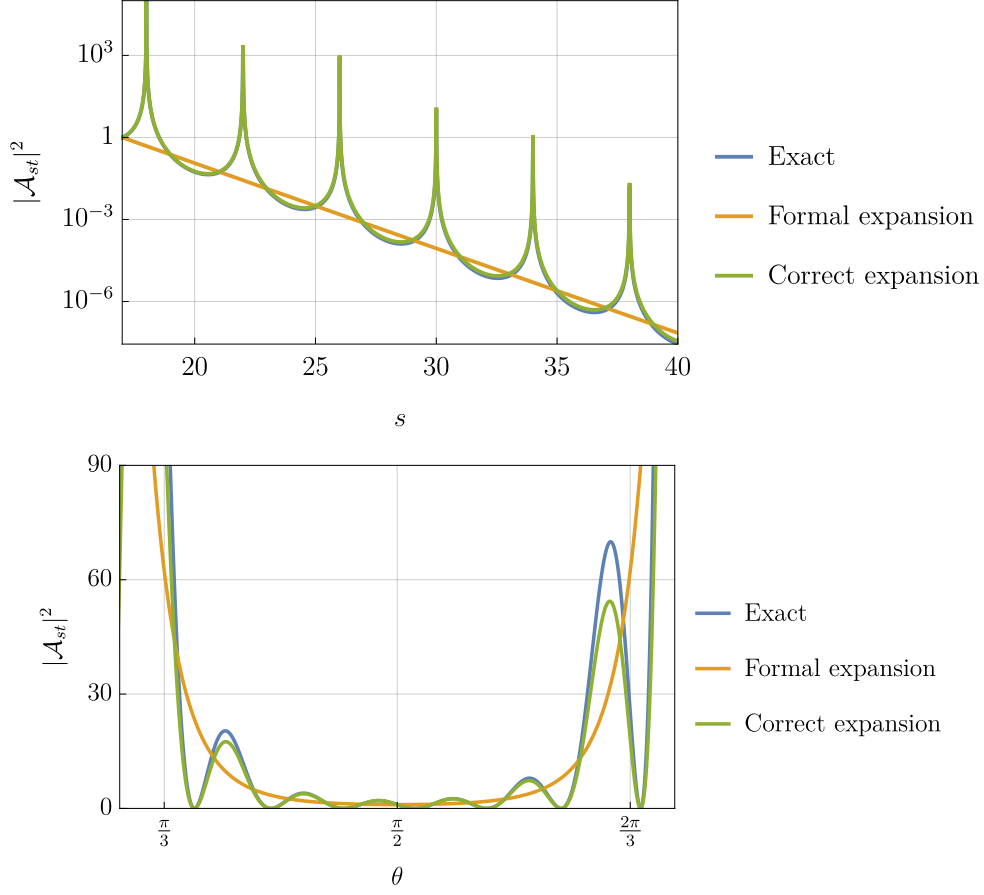


Figure 1. Plots of the Veneziano amplitude (2.1), its formal expansion (2.12), and the correct expansion (2.14) using the reflection formula of the gamma function. All of the amplitudes are normalized at $|\mathbf{p}| = 2.5, \theta = \pi/2$. The formal expansion gives a nice approximation for the size of the Veneziano amplitude, but it misses the poles and zeros of the amplitude. The correct expansion nicely fits the exact amplitude including the location of the poles and zeros.

Stirling's formula is invalid for $z < 0$. However, we have formally used it to expand the gamma functions in (2.1). The appropriate way was to use the reflection formula of the gamma function (2.5), rewriting $\Gamma(z)$ with $\Gamma(1-z)$, and then to apply the Stirling's formula to $\Gamma(1-z)$. In the physical region

$$\begin{aligned}
\mathcal{A}_{st} &= \frac{\sin \pi(\alpha(s) + \alpha(t))}{\sin \pi\alpha(s)} \frac{\Gamma(\alpha(s) + \alpha(t) + 1)\Gamma(-\alpha(t))}{\Gamma(\alpha(s) + 1)} \\
&\sim \frac{\sin \pi(\alpha(s) + \alpha(t))}{\sin \pi\alpha(s)} [\alpha(s)\alpha(t)\alpha(u)]^{-1/2} e^{-\alpha(s) \ln \alpha(s) - \alpha(t) \ln |\alpha(t)| - \alpha(u) \ln |\alpha(u)|} \\
&\sim \frac{\sin \pi(\alpha(s) + \alpha(t))}{\sin \pi\alpha(s)} (stu)^{-3/2} \exp \left[-\frac{1}{2} (s \ln s + t \ln |t| + u \ln |u|) \right]. \quad (2.14)
\end{aligned}$$

Now, we have appropriate poles and zeros. This gives a nice approximation for the Veneziano amplitude, including poles and zeros, as Fig. 1 shows.

This is the point where we should be careful with formal expansions. Stirling's formula is an asymptotic expansion that does not converge for $z^{-1} \rightarrow 0$. Thus, flipping the sign of the argument $z^{-1} \rightarrow -z^{-1}$ by hand does not necessarily give the appropriate analytic continuation. In our case, the form of asymptotic expansion is discontinuously changed from (2.12) to (2.14) by flipping the sign of $\alpha(x)$. Such a discontinuous change of asymptotic expansion is called the Stokes phenomenon¹.

In the next section, we derive this appropriate asymptotic expansion (2.14) purely from saddle point approximation of the worldsheet integral. We point out that there are infinitely many complex saddles contributing to the integral and that they reproduce the appropriate poles and zeros of the Veneziano amplitude.

3 Complex saddles

3.1 Regularization of worldsheet integral

The formal integral (2.8) can be regularized by using the Feynman- $i\epsilon$ prescription [11]. The regularized worldsheet integral is

$$\mathcal{A}_{st}^\epsilon = \int_{C(\epsilon)} dz z^{-\alpha(s)-1-i\epsilon} (1-z)^{-\alpha(t)-1-i\epsilon}. \quad (3.1)$$

Here $|z|, |1-z|$ are promoted to holomorphic variables $z, 1-z$. Each $\alpha(s)$ is shifted by a small imaginary constant, which is in a complete analogy of the ordinal Feynman- $i\epsilon$ prescription in perturbative QFTs. The integration contour is modified to $C(\epsilon)$ from $[0, 1]$. The contour $C(\epsilon)$ is the same one of Figure. 5 of [11], which spirals around $z = 0$ and $z = 1$ infinitely many times to absorb the divergences from these singularities.

3.2 Complex saddles and thimble analysis

Let us rewrite the integral as

$$\mathcal{A}_{st}^\epsilon = \int_{C(\epsilon)} dz e^{-(\alpha(s)+1+i\epsilon) \ln z - (\alpha(t)+1+i\epsilon) \ln(1-z)}. \quad (3.2)$$

Note that the exponent of this integrand has two logarithmic branch cuts from $z = 0, 1$. Thus, we have infinitely many Riemann sheets labeled by two integers (n, m) , where n, m denotes how many times z rotated around the logarithmic singularity at $z = 0, 1$ respectively.

In the previous section, we formally chose the integration contour $[0, 1]$. However, in this case, the integration contour spirals around the logarithmic singularities, running on infinitely many Riemann sheets. Thus, we can no longer ignore other complex saddles on different Riemann sheets.

Solving the saddle point equation, we find infinitely many saddles

$$z_{n,m} = \frac{\alpha(s) + 1 + i\epsilon}{\alpha(s) + \alpha(t) + 2 + 2i\epsilon} \quad \text{on the } (n, m)\text{-th Riemann sheet} \quad (3.3)$$

¹Stokes phenomenon in saddle point approximation is studied in, e.g., [12–14].

such that

$$\ln z_{n,m} = \ln z_{0,0} + 2\pi i n, \quad \ln(1 - z_{n,m}) = \ln(1 - z_{0,0}) + 2\pi i m. \quad (3.4)$$

We have extra phase factors $e^{-2\pi i n(\alpha(s)+1+i\epsilon)-2\pi i m(\alpha(t)+1+i\epsilon)}$ at complex saddles $z = z_{n,m}$ comparing to the trivial saddle $z = z_{0,0}$. Then, the next problem is to identify which complex saddle among these contributes to the regularized worldsheet integral (3.2).

In order to identify contributing saddles, we study thimbles (or steepest descents) of the integral². Denoting the exponent of the integrand by $S(z)$, the thimble $\mathcal{J}_{n,m}$ associated with a saddle $z = z_{n,m}$, or a curve $z = z(s)$ running from a saddle $z = z_{n,m}$, is defined by the following flow equation

$$\frac{dz(s)}{ds} = -\frac{\overline{\partial S(z)}}{\partial z}, \quad z(-\infty) = z_{n,m}. \quad (3.5)$$

By using Cauchy's integral theorem, one may deform the original integration contour $C(\epsilon)$ to a combination of thimbles as

$$\int_{C(\epsilon)} dz e^{S(z)} = \sum_{\{\mathcal{J}_{n,m}\}} (-1)^{(n,m)} \int_{\mathcal{J}_{n,m}} dz e^{S(z)}, \quad (3.6)$$

where $(-1)^{(n,m)} = \pm 1$, called the intersection number, corresponds to the orientation of the thimble $\mathcal{J}_{n,m}$. Along each thimble, the integrand is non-oscillating and decays rapidly. Thus, the integral over each thimble is well approximated by the Gaussian integral

$$\int_{C(\epsilon)} dz e^{S(z)} \sim \sum_{\{z_{n,m}\}} (-1)^{(n,m)} \sqrt{\frac{2\pi}{-S''(z_{n,m})}} e^{S(z_{n,m})}. \quad (3.7)$$

In the following, we identify such a combination of thimbles for physical/unphysical kinematic regions.

Physical region

Suppose that the parameters are in a physical region $|\mathbf{p}|^2 \gg 1$ and $\theta \sim \pi/2$, or equivalently $\alpha(s), \alpha(s) + \alpha(t) \gg 1$ and $\alpha(t) \ll 1$.

The original integration contour $C(\epsilon)$ is depicted as the blue curve in Fig. 2. The contour $C(\epsilon)$ starts from the $(-\infty, 0)$ -th Riemann sheet. It encircles around $z = 0$ in the counterclockwise direction, running on the $(-\infty + 1, 0), \dots, (-1, 0)$ -th Riemann sheets, and appears on the $(0, 0)$ -th Riemann sheet, as the top two panels of Fig. 2 show. Then, the contour $C(\epsilon)$ goes right on the $(0, 0)$ -th Riemann sheet. It encircles around $z = 1$ in the clockwise direction, running on the $(0, -1), \dots, (0, -\infty + 1)$ -th Riemann sheets, and finally ends at the $(0, -\infty)$ -th Riemann sheet.

The original integration contour, the blue curve, is deformed to the orange curve in Fig. 2 by using Cauchy's integral theorem. The deformed contour starts from the $(-\infty, 0)$ -th Riemann sheet, running on infinitely many Riemann sheets, it appears on the $(-1, 0)$ -th

²For thimble analysis in a physics context, see lecture notes e.g. [15, 16]

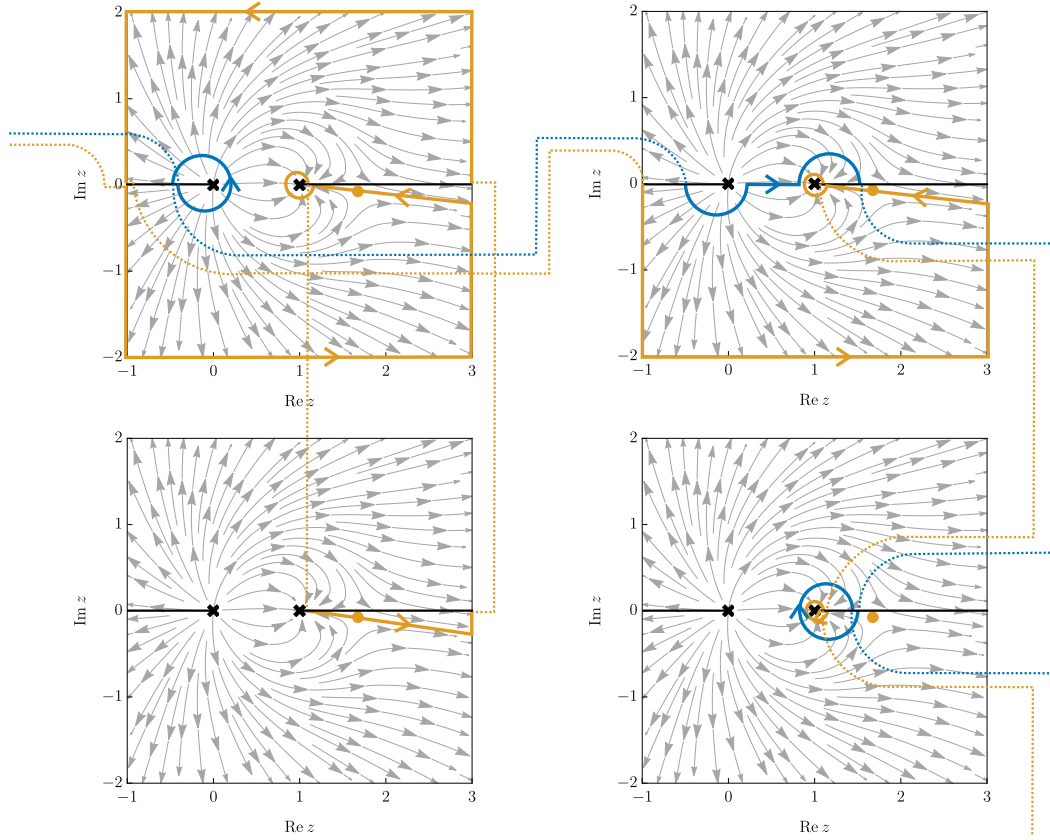


Figure 2. Thimble structure of the regularized worldsheet integral (3.2) in a physical region $|\mathbf{p}| = 2.5$, $\theta = \pi/2$, and $\epsilon = 0.2$. Top-left/right and bottom-left/right panels are the $(-1, 0)$, $(0, 0)$, $(-1, -1)$, $(0, -1)$ -th Riemann sheets, respectively. The blue curve is the original integration contour $C(\epsilon)$, which starts from the $(-\infty, 0)$ -th, running on the $(-1, 0)$, $(0, 0)$, $(0, -1)$ -th, and finally ends at the $(0, -\infty)$ -th Riemann sheet. The gray arrows denote the vector field of the thimble flow equation. Along this vector field, the integrand rapidly decays. The contour $C(\epsilon)$ is deformed to the orange curve, which starts from the $(-\infty, 0)$ -th, running on the $(-1, 0)$, $(-1, -1)$, $(-1, 0)$, $(0, 0)$, $(0, -1)$ -th, and finally ends at the $(0, -\infty)$ -th Riemann sheet. The saddles, depicted as orange bullets, on the $(-\infty, 0)$, $(-\infty, -1)$, \dots , $(-1, 0)$, $(-1, -1)$ -th, and the $(0, 0)$ -th Riemann sheets contribute the integral.

Riemann sheet, as the top-left panel of Fig. 2 shows. The deformed contour passes through a saddle, an orange bullet, on the $(-1, 0)$ -th Riemann sheet. It goes down to the $(-1, -1)$ -th Riemann sheet, as the bottom-left panel of Fig. 2 shows, passing through a saddle on the $(-1, -1)$ -th Riemann sheet. It runs again on the $(-1, 0)$ -th Riemann sheet, appearing on the $(0, 0)$ -th Riemann sheet. The contour passes through a saddle on the $(0, 0)$ -th Riemann sheet, going down to the $(0, -1)$ -th Riemann sheet. It runs on infinitely many Riemann sheets, ending at the $(0, -\infty)$ -th Riemann sheet.

Such a deformed contour can be found by following the gray arrows in Fig. 2, that is,

the gradient of the flow equation (3.5) such that

$$\left(\operatorname{Re} \left[-\frac{\partial S(z)}{\partial z} \right], \operatorname{Im} \left[-\frac{\partial S(z)}{\partial z} \right] \right). \quad (3.8)$$

Along this vector field, the integrand rapidly decreases. Thus, if we drag the original integration contour along the vector field, we obtain curves that give vanishing contributions around singularities or infinities, or curves that give finite contributions around saddles. In this physical case, since $\alpha(s), \alpha(s) + \alpha(t) \gg 1$ and $\alpha(t) \ll 1$, the integral around a singularity $z = 1$ and around infinities $|z| = \infty$ gives vanishing contributions, but the integral along thimbles gives finite contributions.

In summary, we find that infinitely many saddles on the

$$(-\infty, 0), (-\infty, -1), \dots, (-1, 0), (-1, -1), (0, 0)\text{-th Riemann sheets} \quad (3.9)$$

contribute to the integral. Summing all of these contributions, and noting that the orientation of the thimbles on the $(*, -1)$ -th Riemann sheets are flipped, we obtain

$$\begin{aligned} \mathcal{A}_{st}^\epsilon &= \int_{C(\epsilon)} dz e^{S(z)} \\ &\sim \sqrt{\frac{2\pi}{-S''(z_{0,0})}} e^{S(z_{0,0})} + \sum_{n \leq -1} \sqrt{\frac{2\pi}{-S''(z_{n,0})}} e^{S(z_{n,0})} - \sum_{n \leq -1} \sqrt{\frac{2\pi}{-S''(z_{n,-1})}} e^{S(z_{n,-1})} \\ &= \left[1 + \sum_{n \leq -1} e^{-2\pi i n(\alpha(s)+1+i\epsilon)} - \sum_{n \leq -1} e^{-2\pi i n(\alpha(s)+1+i\epsilon) - 2\pi i(-1)(\alpha(t)+1+i\epsilon)} \right] \\ &\quad \times \sqrt{\frac{2\pi}{-S''(z_{0,0})}} e^{S(z_{0,0})} \\ &\sim \frac{1 - e^{2\pi i(\alpha(s)+\alpha(t)+2+2i\epsilon)}}{1 - e^{2\pi i(\alpha(s)+1+i\epsilon)}} \sqrt{\frac{2\pi}{-S''(z_{0,0})}} e^{S(z_{0,0})} \\ &\sim \frac{\sin \pi(\alpha(s) + \alpha(t))}{\sin \pi \alpha(s)} \left(\frac{\alpha(u)^3}{\alpha(s)\alpha(t)} \right)^{-1/2} e^{-(\alpha(s)+1) \ln \alpha(s) - (\alpha(t)+1) \ln |\alpha(t)| - (\alpha(u)-1) \ln |\alpha(u)|} \\ &\sim \frac{\sin \pi(\alpha(s) + \alpha(t))}{\sin \pi \alpha(s)} (stu)^{-3/2} \exp \left[-\frac{1}{2} (s \ln s + t \ln |t| + u \ln |u|) \right]. \quad (3.10) \end{aligned}$$

This agrees with the correct asymptotic expansion (2.14) obtained by analytic continuation of the gamma function. It is remarkable that the infinitely many complex saddles reproduce the appropriate poles and zeros of the amplitude while the trivial saddle at $z = z_{0,0}$ alone gives the same result as the formal saddle approximation (2.8).

Unphysical region

Suppose that the parameters are in fictitious unphysical region $\alpha(s), \alpha(t), \alpha(s) + \alpha(t) \ll 1$. In this case, the thimble structure discontinuously changes as follows, compared to the previous physical case.

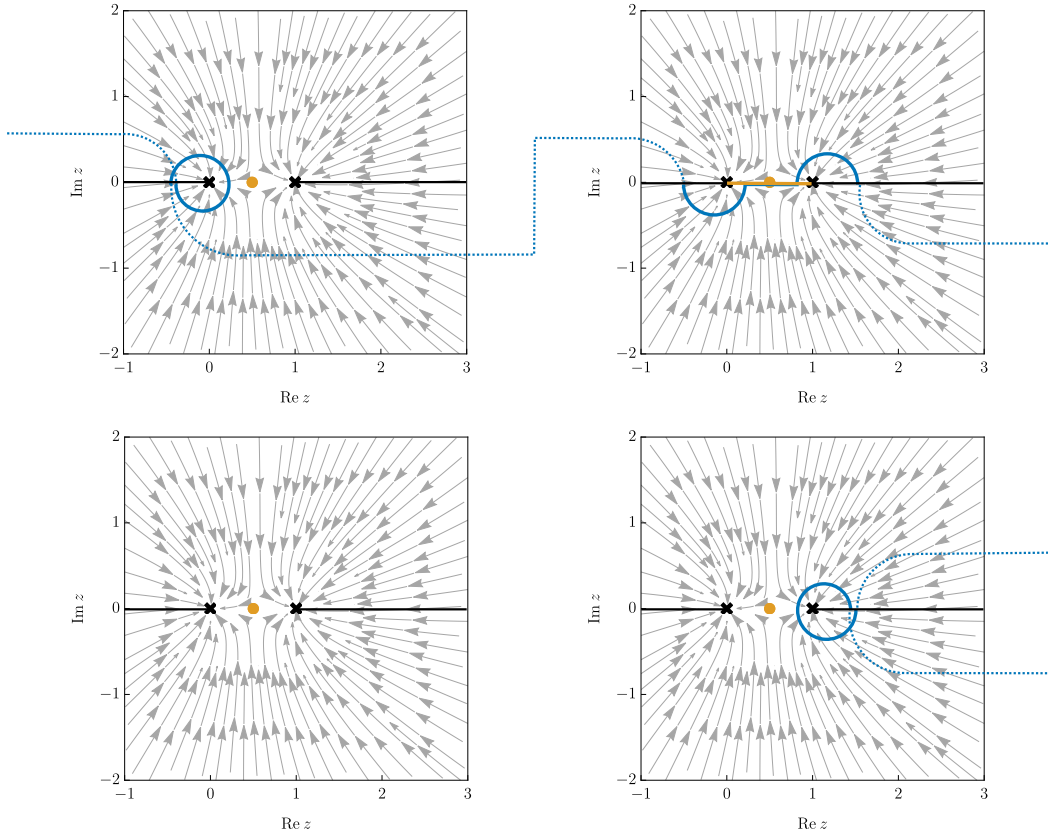


Figure 3. Thimble structure of the regularized worldsheet integral (3.2) in unphysical region $\alpha(s) = \alpha(t) = -5.0$, and $\epsilon = 0.2$. Top-left/right and bottom-left/right panels are the $(-1, 0)$, $(0, 0)$, $(-1, -1)$, $(0, -1)$ -th Riemann sheets respectively. The blue curve is the original integration contour $C(\epsilon)$, which starts from the $(-\infty, 0)$ -th, running on the $(-1, 0)$, $(0, 0)$, $(0, -1)$ -th, and finally ends at the $(0, -\infty)$ -th Riemann sheet. The gray arrows denote the vector field of the thimble flow equation. Along this vector field, the integrand rapidly decays. The contour $C(\epsilon)$ is deformed to the orange curve, which runs within an interval $[0, 1]$ on the $(0, 0)$ -th Riemann sheet. A single saddle, depicted as an orange bullet, on the $(0, 0)$ -th Riemann sheet contributes the integral.

The original integration contour $C(\epsilon)$ is the same as the previous physical case. It starts from the $(-\infty, 0)$ -th Riemann sheet, running on the $(-\infty + 1, 0), \dots, (-1, 0)$ -th Riemann sheets, and appears on the $(0, 0)$ -th Riemann sheet. It goes down to the $(0, -1)$ -th Riemann sheet, finally ending at the $(0, -\infty)$ -th Riemann sheet.

However, in this unphysical case, we cannot deform the original integration contour as in the physical case. As depicted in Fig. 3, the vector field of the thimble equation flows into the logarithmic singularities at $z = 0, 1$. Thus, if we drag the original integration contour to infinity as in the previous physical case, it gives infinite uncontrollable contributions. Instead, we should shrink the spiral contour and deform it to the interval $[0, 1]$ on the $(0, 0)$ -th Riemann sheet as Fig. 3. The integral around $z = 0, 1$ gives vanishing contributions.

Thus, we find that the integral is dominated by a single saddle on the

$$(0, 0)\text{-th Riemann sheet.} \quad (3.11)$$

Finally, we obtain

$$\begin{aligned} \mathcal{A}_{st}^\epsilon &= \int_{C(\epsilon)} dz e^{S(z)} \\ &\sim \sqrt{\frac{2\pi}{-S''(z_{0,0})}} e^{S(z_{0,0})} \\ &\sim \left(\frac{\alpha(u)^3}{\alpha(s)\alpha(t)} \right)^{-1/2} e^{-(\alpha(s)+1)\ln\alpha(s) - (\alpha(t)+1)\ln\alpha(t) - (\alpha(u)-1)\ln\alpha(u)} \\ &\sim (stu)^{-3/2} \exp \left[-\frac{1}{2} (s \ln s + t \ln t + u \ln u) \right]. \end{aligned} \quad (3.12)$$

This is the result of the formal expansion (2.11). This result is in contrast to the previous physical region. In the unphysical region, only the single saddle on the $(0, 0)$ -th Riemann sheet contributes to the integral. Then, the amplitude is only exponentially suppressed. However, in the physical region, the location of saddles and thimble structures are discontinuously changed. Infinitely many extra saddles on the $(-\infty, 0), (-\infty, -1), \dots, (-1, 0), (-1, -1)$ -th Riemann sheets contribute to the integral, reproducing the poles and zeros of the original amplitude.

4 Discussions

The infinitely many complex saddles we have found are not just technical subjects of regularization and approximations. Rather, they have physical significance in the following sense.

4.1 Stringy excitations

The poles of the Veneziano amplitude stem from the gamma function $\Gamma(-\alpha(s))$, which are associated with stringy excitations labeled by $\alpha(s) \in \mathbb{Z}_{\geq}$. In this paper, we have shown that the poles are reproduced from infinitely many complex saddles. The infinitely many complex saddles we have found can be divided into two classes: the ones on the $(n, 0)$ -th with $n \leq 0$, and the $(n-1, -1)$ -th with $n \leq 0$.

Summing all of the the extra phase factors of saddles on the $(n, 0)$ -th Riemann sheets, we have

$$\sum_{n \leq 0} e^{-2\pi i n(\alpha(s)+1+i\epsilon)} = \frac{1}{1 - e^{2\pi i(\alpha(s)+1+i\epsilon)}}. \quad (4.1)$$

Similarly for the $(n-1, -1)$ -th Riemann sheets, we have

$$-\sum_{n \leq 0} e^{-2\pi i n(\alpha(s)+1+i\epsilon) - 2\pi i(-1)(\alpha(s)+1+i\epsilon) - 2\pi i(-1)(\alpha(t)+1+i\epsilon)} = -\frac{e^{2\pi i(\alpha(s)+\alpha(t)+2+i\epsilon)}}{1 - e^{2\pi i(\alpha(s)+1+i\epsilon)}}. \quad (4.2)$$

Each class contributes to the s -channel poles of the amplitude.

Combining these, we obtain a factor

$$\frac{1 - e^{2\pi i(\alpha(s)+\alpha(t)+2+i\epsilon)}}{1 - e^{2\pi i(\alpha(s)+1+i\epsilon)}}, \quad (4.3)$$

whose numerator gives zeros. This is also associated with stringy excitations $\alpha(s) \in \mathbb{Z}_{\geq}$.

4.2 Semi-classical paths

The Veneziano amplitude is expressed in path integral formalism as

$$\int \mathcal{D}X \prod_{j=1}^4 e^{ip_j X(z_j)} e^{-\int d^2z (\partial X)^2}. \quad (4.4)$$

Regarding each exponent of the vertex operators as a source, and solving the equation of motion, we obtain a semi-classical path of a string

$$X(z) = \sum_j (-ip_j) \ln |z - z_j|. \quad (4.5)$$

In our setup, the vertices are fixed as $z_1 = z$, $z_2 = 0$, $z_3 = 1$, $z_4 = \infty$, and variables $|z|$, $|z - 1|$ have been promoted to holomorphic variables in order to find complex saddles. Thus, the semi-classical path of a string reduces to

$$X(z) = -ip_2 \ln z - ip_3 \ln(z - 1). \quad (4.6)$$

Around the vertex operator at $z = 0$, the variable z is expressed as $z = e^{\tau+i\sigma}$, where τ is the Euclidean time of a string worldsheet.

The Feynman- $i\epsilon$ prescription in string theory is regarded as an analytic continuation to Lorentzian time [11, 17–19]. The formal integration contour $z : 0 \rightarrow 1$ in (2.8) corresponds to Euclidean time development $\tau : -\infty \rightarrow 0$. But in the Feynman- $i\epsilon$ prescription, the formal integration contour is bent at a point $z = z_*$ close to the origin as

$$\tau \rightarrow \tau + it \quad (4.7)$$

to encircle around the branch cut singularity. Here, t is interpreted as Lorentzian time of string worldsheet. The difference in the position of a string is indeed real as

$$X(z) - X(z_*) = p_2 t. \quad (4.8)$$

In this paper, we have found infinitely many complex saddles. Each complex saddle $z = z_{n,m}$ corresponds to a semi-classical string at $X = X(z_{n,m})$. Its difference from the trivial saddle is

$$X(z_{n,m}) - X(z_{0,0}) = p_2(2\pi n) + p_3(2\pi m). \quad (4.9)$$

Recall that a class of infinitely many saddles on the $(n, 0)$ -th Riemann sheets with $n \leq 0$ combined gives the s -channel poles as (4.1) shows. Using the semi-classical picture (4.9),

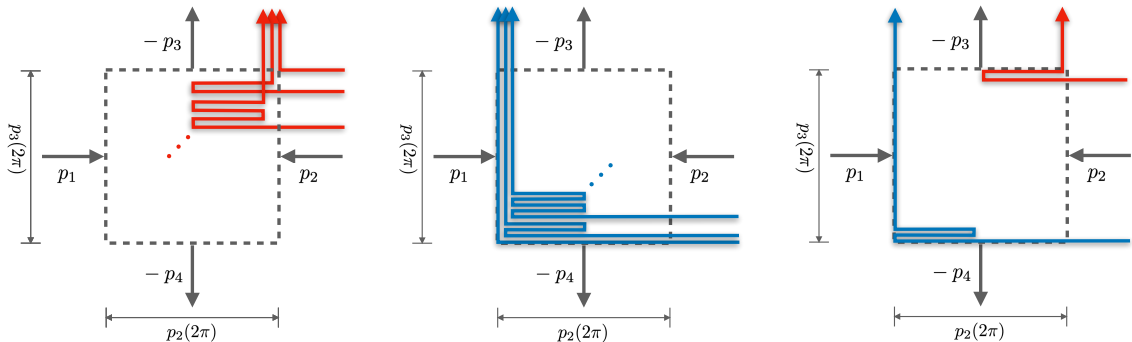


Figure 4. Visualization of semi-classical interpretation of the Veneziano amplitude in Lorentzian signature. External lines are incoming/outgoing momenta, and dotted squared regions are scattering regions. The left panel visualizes infinitely many semi-classical paths, depicted as red lines, with extra optical length $p_2(2\pi n)$, $n \leq 0$ interfering constructively, generating the poles (4.1). Similarly, the middle panel visualizes infinitely many semi-classical paths, depicted as blue lines, with extra optical length $p_3(2\pi n) + p_2(-2\pi) + p_3(-2\pi)$, $n \leq 0$ interfering constructively, generating the poles (4.2). The right panel visualizes a pair of semi-classical paths with extra optical length $p_2(2\pi n)$ and $p_2(2\pi n) + p_2(-2\pi) + p_3(-2\pi)$ interfering destructively, generating the zeros (4.3).

we can interpret that the poles are generated by infinitely many string paths with extra optical length $p_2(2\pi n)$, $n \leq 0$, interfering constructively.

Similarly, another pole structure of (4.2), associated with the $(n-1, -1)$ -th Riemann sheets with $n \leq 0$, is generated from infinitely many string paths with extra optical length $p_2(2\pi n) + p_2(-2\pi) + p_3(-2\pi)$, $n \leq 0$, interfering constructively.

Also recall that a pair of complex saddles on the $(n, 0)$, $(n-1, -1)$ -th Riemann sheets for each $n \leq 0$ gives the zeros of the amplitude as (4.3) shows. Similarly, using the semi-classical picture (4.9), we can interpret that the zeros are generated by a pair of two string paths with extra optical length $p_2(2\pi n)$ and $p_2(2\pi n) + p_2(-2\pi) + p_3(-2\pi)$, interfering destructively. These semi-classical paths in Lorentzian signature are visualized in Fig. 4.

We should remark that such an interpretation of poles and zeros as interference of semi-classical paths emerged from analytic continuation. Originally, string amplitude is defined as an integral on a single Euclidean worldsheet. However, the integral is actually a formal one since it diverges at its logarithmic singularities. By introducing the Feynman- $i\epsilon$ prescription, we can analytically continue back to the Lorentzian signature. The new integration contour of the Feynman- $i\epsilon$ prescription encircles around the logarithmic singularities infinitely many times. Then, string amplitude is no longer living on a single Riemann sheet³. We have shown that by deforming the new integration contour, infinitely

³The authors of [19] already pointed out that the worldsheet turns asymptotically into a collection of worldlines. Their interpretation is slightly different from our interpretation; they provided an interpretation for spiral integration contours around the logarithmic singularities while we provided for deformed integration contours and complex saddles. Our deformed integration contours give finite contribution only around

many complex saddles on different Riemann sheets contribute to the Veneziano amplitude. Contribution from each complex saddle is interpreted as a semi-classical path of a string with different optical lengths as (4.9) indicates. Then, the poles and zeros are interpreted as interference of such a collection of semi-classical string paths⁴.

Interference of semi-classical paths affects scattering amplitude, which is a physical observable in principle. In this sense, the infinitely many complex saddles have physical significance.

We also note that interference of semi-classical paths is a unique feature of strings. The reason why we have different optical paths is because (4.6) is expressed with a logarithm, which is a 2-dimensional Green function. Contrary to a string, in the first quantization formalism of a point-particle, we have instead an 1-dimensional Green function, which is just a linear function. Thus, point-particles cannot interfere by themselves.

4.3 Unitarity and locality

Unitarity of the Veneziano amplitude constraints the residue of the s -channel poles [21, 22]. The residue of the Veneziano amplitude (2.1) around $s \sim 2n - 2$ is

$$-\text{Res}_n = \frac{2}{\Gamma(n+1)} \frac{\Gamma(n+2+t/2)}{\Gamma(2+t/2)}. \quad (4.10)$$

Denoting $x = \cos \theta$, the residue can be expanded in the Gegenbauer polynomials $C_j^\alpha(x)$, which is generalizations of the Legendre polynomials, as

$$-\text{Res}_n = \sum_{j=0}^n a_{n,j} C_j^\alpha(x), \quad \alpha = \frac{D-3}{2}. \quad (4.11)$$

Partial wave unitarity demands that all of the coefficients $a_{n,j}$ are positive. For example, at the critical spacetime dimension $D = 26$,

$$\begin{aligned} -\text{Res}_0 &= 2 &&= 2C_0^\alpha(x) \\ -\text{Res}_1 &= 4x &&= \frac{4}{23}C_1^\alpha(x) \\ -\text{Res}_2 &= -\frac{1}{4} + \frac{25}{4}x^2 &&= \frac{1}{46}C_2^\alpha(x) \\ -\text{Res}_3 &= -x + 9x^3 &&= \frac{2}{575}C_3^\alpha(x) \\ -\text{Res}_4 &= \frac{3}{64} - \frac{245}{96}x^2 + \frac{2401}{192}x^4 &&= \frac{2401}{3601800}C_4^\alpha(x) + \frac{49}{400200}C_2^\alpha(x) + \frac{1}{2700}C_0^\alpha(x) \end{aligned} \quad (4.12)$$

All of these coefficients are indeed positive.

From the formal real saddle approximation (2.11), we cannot discuss partial wave unitarity since it does not know the location of the poles. In contrast, our complex saddle approximation knows the appropriate location of poles. In the asymptotic region $\alpha(s) \gg 1$ with $x = \cos \theta \sim 0$, we can obtain the residue approximately. For example,

$$\begin{aligned} -\text{Res}_2 &\sim -0.250 + 6.71x^2 + \mathcal{O}(x^4) \\ -\text{Res}_3 &\sim -0.900x + 9.27x^3 + \mathcal{O}(x^6) \\ -\text{Res}_4 &\sim +0.0428 - 2.37x^2 + 13.7x^4 + \mathcal{O}(x^8) \end{aligned}, \quad (4.13)$$

complex saddles in the high energy limit.

⁴Such an interference of different optical paths is analogous to the standard double-slit experiment [20]. It is interesting that a single string looks like a double-slit due to its structure in the Lorentzian signature.

where the amplitude is normalized so that the constant term of Res_2 is $1/4 = 0.250$. The other coefficients nicely match the exact value of the residue (4.12). Thus, the complex saddles know partial wave unitarity of the amplitude in the asymptotic region.

We should also note that our complex saddle approximation is not inconsistent with the previous studies on unitarity and locality. Although complex saddles give extra information about the angle dependence and poles/zeros of amplitudes, they do not alter the size of amplitude at a fixed angle, as Fig. 1 shows. If this was the case for higher genus corrections, our complex saddle approximation does not conflict with [6], in which amplitudes were evaluated at the dominant saddle point at a fixed angle.

5 Conclusion

In this paper, we have studied complex saddles and the thimble structure of the Veneziano amplitude. We have shown that infinitely many complex saddles contribute to the amplitude, reproducing the appropriate poles and zeros. The location of the poles and zeros matches an analytic continuation of the Veneziano amplitude from an unphysical region to a physical region.

Our result reproduces the appropriate angle dependence in the asymptotic region while preserving the universal fall-off behavior of the amplitude. Thus, our result provides extra information for the amplitude, being consistent with previous studies.

Complex saddles have physical significance. They are never technical artifacts of regularization or approximation. The infinitely many complex saddles are associated with stringy excitations, semi-classical paths of a string in the Lorentzian signature, and unitarity in the asymptotic region.

In particular, it is remarkable that complex saddles allow a semi-classical picture of string scatterings. Originally, tree-level string amplitude is defined on a single Euclidean worldsheet. However, after analytically continuing back to the Lorentzian signature, we have infinitely many Riemann sheets. Complex saddles on different Riemann sheets are interpreted as semi-classical paths of a string with different optical lengths. Their interference generates the poles and zeros of amplitude.

It will be worthwhile to extend our results to higher genus corrections. Our results do not ruin the previous results [1–6], rather, add extra information from complex saddles. We expect that we can go higher genus corrections by generalizing our result in a natural way. In particular, it will be valuable to study how the modular invariance of string worldsheets is reflected in the thimble structure.

It will also be interesting to explore what complex saddles tell us more about the space-time structure in the high energy limit. Our complex saddle approximation gives more information about the angle dependence and semi-classical string optical paths. Semi-classical paths of a string may give a nice analogy to chaotic particle trajectories in classical scatterings. We hope that we can find chaos in string scatterings and evaluate their chaoticity quantitatively [23–28].

Acknowledgments

The author would like to thank Koji Hashimoto for valuable comments on his manuscript. Also the author would like to thank the Yukawa Institute for Theoretical Physics at Kyoto University. Discussions during the YITP workshop “Strings and Fields 2023” were useful to complete this work. The work of T. Y. was supported in part by JSPS KAKENHI Grant No. JP22H05115 and JP22KJ1896.

A Thimble analysis

In this section, we summarize a thimble analysis of special functions whose asymptotic behaviors can be analyzed by the same method as the Feynman- $i\epsilon$ prescription [11].

A.1 Gamma function

Let us define a regularized version of the gamma function by

$$\Gamma^\epsilon(z) := \int_{C(\epsilon)} dt t^{z-1} e^{-t}. \quad (\text{A.1})$$

The integration contour runs from $t = 0$ to $t = \infty$, but it encircles around $t = 0$ in the counterclockwise direction infinitely many times, as depicted in Fig 5 and 6, in order to absorb divergence. The saddles of the regularized version of the gamma function are

$$t_n = z - 1 - i\epsilon \quad \text{on the } n\text{-th Riemann sheet}, \quad (\text{A.2})$$

such that

$$\ln t_n = \ln t_0 + 2\pi i n. \quad (\text{A.3})$$

Positive case

In a case $z > 0$, the original integration contour, the blue curve, is deformed to the orange curve in Fig. 5 by using Cauchy’s integral theorem. Since the integral vanishes around $t = 0$, we can shrink the integration contour to the origin.

The deformed contour, the orange curve, runs from the origin to infinity on the 0-th Riemann sheet. Thus, only the trivial saddle on the 0-th Riemann sheet contributes to the integral

$$\begin{aligned} \Gamma^\epsilon(z) &= \int_{C(\epsilon)} dt e^{S(t)} \\ &\sim \sqrt{\frac{2\pi}{-S''(t_0)}} e^{S(t_0)} \\ &\sim e^{(z-1/2) \ln z - z + \ln \sqrt{2\pi}}. \end{aligned} \quad (\text{A.4})$$

This is the well-known Stirling’s formula.

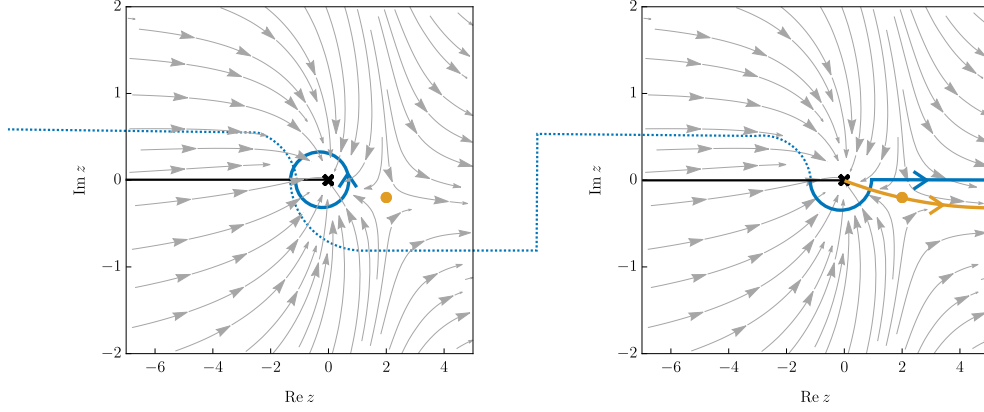


Figure 5. Thimble structure of the regularized version of the gamma function when $z = 3$ and $\epsilon = 0.2$. The left/right panels are the $-1, 0$ -th Riemann sheets respectively. The blue curve is the original integration contour $C(\epsilon)$, which starts from the $-\infty$ -th Riemann sheet, and finally ends at the infinity of the 0 -th Riemann sheet. The gray arrows denote the vector field of the thimble flow equation. Along this vector field, the integrand rapidly decays. The contour $C(\epsilon)$ is deformed to the orange curve, which starts from the origin of the 0 -th Riemann sheet, and ends at the infinity of the same sheet. A single saddle, depicted as an orange bullet, on the 0 -th Riemann sheet contributes to the integral.

Negative case

In a case $z < 0$, the thimble structure discontinuously changes as depicted in Fig. 6. Since the integral diverges around $t = 0$, the integration contour is deformed away from the origin. The deformed contour runs around the infinities or passes through complex saddles on different Riemann sheets.

The deformed contour starts from the $(-\infty)$ -th Riemann sheet. It goes up through infinitely many Riemann sheets, appearing on the (-1) -th Riemann sheet, as the left panel of Fig. 6 shows. It passes through a saddle, going around the infinity in the counter-clockwise direction, it appears on the 0 -th Riemann sheet. It passes through a saddle on the 0 -th Riemann sheet, then goes away to infinity. Thus, infinitely many saddles on the $-\infty, \dots, -1, 0$ -th Riemann sheets contribute to the integral

$$\begin{aligned}
\Gamma^\epsilon(z) &= \int_{C(\epsilon)} dt e^{S(t)} \\
&\sim \sum_{n \leq 0} \sqrt{\frac{2\pi}{-S''(t_n)}} e^{S(t_n)} \\
&= \left(\sum_{n \leq 0} e^{2\pi i n(z-1-i\epsilon)} \right) \sqrt{\frac{2\pi}{-S''(t_0)}} e^{S(t_0)} \\
&\sim \frac{1}{1 - e^{-2\pi i z}} e^{(z-1/2) \ln z - z + \ln \sqrt{2\pi}}.
\end{aligned} \tag{A.5}$$

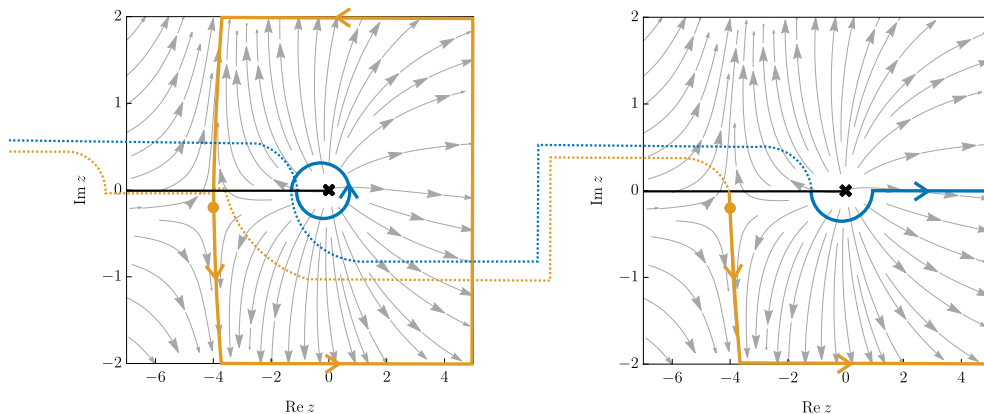


Figure 6. Thimble structure of the regularized version of the gamma function when $z = -3$ and $\epsilon = 0.2$. The left/right panels are the $-1, 0$ -th Riemann sheets respectively. The blue curve is the original integration contour $C(\epsilon)$, which starts from the $-\infty$ -th Riemann sheet, and finally ends at the infinity of the 0 -th Riemann sheet. The gray arrows denote the vector field of the thimble flow equation. Along this vector field, the integrand rapidly decays. The contour $C(\epsilon)$ is deformed to the orange curve, which starts from the $-\infty$ -th Riemann sheet, running through the $-\infty + 1, \dots, -1$ -th, and finally ends at the infinity of the 0 -th Riemann sheet. Infinitely many saddles, depicted as orange bullets, on the $-\infty, \dots, 0$ -th Riemann sheets contribute to the integral.

This agrees with the appropriate asymptotic expansion obtained by an analytic continuation using the reflection formula

$$\Gamma(z) = \frac{\pi}{\sin \pi z} \frac{1}{\Gamma(1-z)}, \quad (\text{A.6})$$

and by expanding $\Gamma(1-z)$ using Stirling's formula.

References

- [1] D.J. Gross and P.F. Mende, *The High-Energy Behavior of String Scattering Amplitudes*, *Phys. Lett. B* **197** (1987) 129.
- [2] D.J. Gross and P.F. Mende, *String Theory Beyond the Planck Scale*, *Nucl. Phys. B* **303** (1988) 407.
- [3] D.J. Gross, *High-Energy Symmetries of String Theory*, *Phys. Rev. Lett.* **60** (1988) 1229.
- [4] D.J. Gross, *Strings at superPlanckian energies: In search of the string symmetry*, *Phil. Trans. Roy. Soc. Lond. A* **329** (1989) 401.
- [5] D.J. Gross and J.L. Manes, *The High-energy Behavior of Open String Scattering*, *Nucl. Phys. B* **326** (1989) 73.
- [6] P.F. Mende and H. Ooguri, *Borel Summation of String Theory for Planck Scale Scattering*, *Nucl. Phys. B* **339** (1990) 641.
- [7] C.-T. Chan, J.-C. Lee and Y. Yang, *Notes on high energy bosonic closed string scattering amplitudes*, *Nucl. Phys. B* **749** (2006) 280 [[hep-th/0604122](#)].

- [8] H. Kawai, D.C. Lewellen and S.H.H. Tye, *A Relation Between Tree Amplitudes of Closed and Open Strings*, *Nucl. Phys. B* **269** (1986) 1.
- [9] G. Veneziano, *Construction of a crossing - symmetric, Regge behaved amplitude for linearly rising trajectories*, *Nuovo Cim. A* **57** (1968) 190.
- [10] C.-T. Chan, P.-M. Ho and J.-C. Lee, *Ward identities and high-energy scattering amplitudes in string theory*, *Nucl. Phys. B* **708** (2005) 99 [[hep-th/0410194](#)].
- [11] E. Witten, *The Feynman ie in String Theory*, *JHEP* **04** (2015) 055 [[1307.5124](#)].
- [12] M.V. Berry and C.J. Howls, *Hyperasymptotics for integrals with saddles*, *Proceedings: Mathematical and Physical Sciences* **434** (1991) 657.
- [13] W. Boyd, *Error bounds for the method of steepest descents*, *Proceedings of the Royal Society A: Mathematical and Physical Sciences* **440** (1993) 493 .
- [14] W. Boyd, *Gamma function asymptotics by an extension of the method of steepest descents*, *Proceedings of the Royal Society A: Mathematical and Physical Sciences* **447** (1994) 609 .
- [15] M. Mariño, *Lectures on non-perturbative effects in large N gauge theories, matrix models and strings*, *Fortsch. Phys.* **62** (2014) 455 [[1206.6272](#)].
- [16] M. Mariño, *Instantons and Large N : An Introduction to Non-Perturbative Methods in Quantum Field Theory*, Cambridge University Press (2015).
- [17] L. Eberhardt and S. Mizera, *Evaluating one-loop string amplitudes*, *SciPost Phys.* **15** (2023) 119 [[2302.12733](#)].
- [18] L. Eberhardt and S. Mizera, *Unitarity cuts of the worldsheet*, *SciPost Phys.* **14** (2023) 015 [[2208.12233](#)].
- [19] S. Caron-Huot, M. Giroux, H.S. Hannesdottir and S. Mizera, *Crossing beyond scattering amplitudes*, [2310.12199](#).
- [20] K. Hashimoto, Y. Matsuo and T. Yoda, *String is a double slit*, *PTEP* **2023** (2023) 043B04 [[2206.10951](#)].
- [21] N. Arkani-Hamed, L. Eberhardt, Y.-t. Huang and S. Mizera, *On unitarity of tree-level string amplitudes*, *JHEP* **02** (2022) 197 [[2201.11575](#)].
- [22] P. Maity, *Positivity of the Veneziano amplitude in $D = 4$* , *JHEP* **04** (2022) 064 [[2110.01578](#)].
- [23] D.J. Gross and V. Rosenhaus, *Chaotic scattering of highly excited strings*, *JHEP* **05** (2021) 048 [[2103.15301](#)].
- [24] V. Rosenhaus, *Chaos in a Many-String Scattering Amplitude*, *Phys. Rev. Lett.* **129** (2022) 031601 [[2112.10269](#)].
- [25] M. Bianchi, M. Firrotta, J. Sonnenschein and D. Weissman, *Measure for Chaotic Scattering Amplitudes*, *Phys. Rev. Lett.* **129** (2022) 261601 [[2207.13112](#)].
- [26] M. Firrotta, *The chaotic emergence of thermalization in highly excited string decays*, *JHEP* **04** (2023) 052 [[2301.04069](#)].
- [27] M. Bianchi, M. Firrotta, J. Sonnenschein and D. Weissman, *Measuring chaos in string scattering processes*, *Phys. Rev. D* **108** (2023) 066006 [[2303.17233](#)].
- [28] K. Hashimoto, Y. Matsuo and T. Yoda, *Transient chaos analysis of string scattering*, *JHEP* **11** (2022) 147 [[2208.08380](#)].